Experimental study of a particulate turbulent confined jet by optical methods

L. Vignal*, L. Ben */**, V. Roig*, R. Bazile*, J. Borée***

* Institut de Mécanique des Fluides de Toulouse, UMR 5502 CNRS-INPT-UPS,

Allée du Prof. Camille Soula, 31400 Toulouse, France

** CEMAGREF, Unité Temo TAPV, Montpellier, France

*** Laboratoire d'Etudes Aérodynamiques, ENSMA Poitiers, France

ABSTRACT

A new experimental set-up has been developed to improve the understanding of dispersion in a dilute two-phase flow. A confined jet flow (figure a) is used to generate quasi homogeneous and isotropic turbulence. An original seeding system injects glass particles (40/50µm) in the flow. Particle and gas velocities are measured simultaneously by a PIV/PTV algorithm. Accuracy of 2D2C PIV measurements in isotropic turbulent flow is tested with synthetic images created from DNS calculations. Cell shifting and deformation are used for PIV calculation, optimal mesh size, seeding diameter and seeding displacement are evaluated. Effects of the third component and of the laser sheet energy shape are also estimated. The cut-off effect due to the presence of particles on the images upon the measured PIV spectrum in the gas phase is tested. The characterisation of the turbulence of the gas phase (figure b) gives good agreement with the results obtained by Risso & Fabre (1997). Preliminary results concerning the dynamics of the dispersed phase are discussed (figure c).

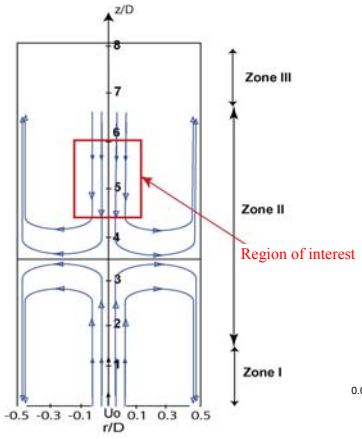

Figure a. Schematic flow configuration in the tube

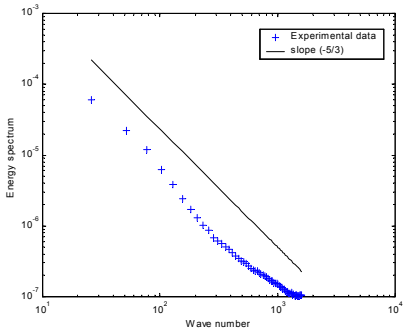

Figure b. Energy spectrum in the gas phase in the region of interest

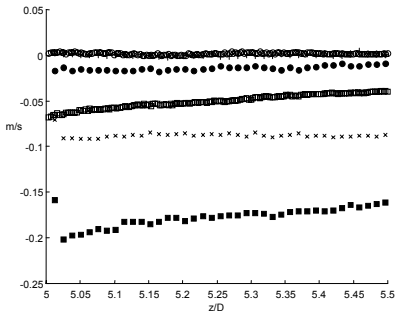

Figure c. Longitudinal evolution of the mean particles velocities

run 1 : □ $\overline{U_{zg}}$; ○ $\overline{U_{yg}}$; run 2: *x* $\overline{U_{zp}}$; + $\overline{U_{yp}}$;

run 3 : ■ $\overline{U_{zp}}$; • $\overline{U_{yp}}$

1. INTRODUCTION

The aim of this experimental study is to improve the understanding of the physics of turbulent particulate two-phase flows. Even if a lot of studies has been devoted to such flows, some questions are still unresolved. Two-way coupling and modification of the turbulence by the dispersed phase may deeply affect the dynamics of such flows. Modification of the relative motion or inertial effects modifying the turbulent dispersion can also be important. These effects can lead for example to "preferential concentration", a phenomenon which has already been discussed by several authors (Squires *et al.* 1990, Eaton *et al.* 1994, Fessler *et al.* 1994, Février 2000). Whatever the great amount of work devoted to such studies, experiments in controlled flows are needed, and detailed measurements of conditional statistics (statistical fluid/particle correlations at one point), or of spatial fluid/particle correlations can help to discuss recent modelling mainly based on a great amount of numerical work (Février 2000, Février *et al.* 2001, Fede *et al.* 2004). In the present study, we have chosen to investigate an original turbulent flow where homogeneity and isotropy properties greatly simplify the flow dynamics. In particulate flows, the extend of the various turbulent length scales involved in the dynamics of the fluctuating motions is quite important. We want to access to a precise experimental description up to the finest scales. So, while developing a PIV/PTV algorithm to measure simultaneously the velocity fields of both phases, we first focussed on a careful check of the performances of PIV measurements. In this paper we present the analysis of the PIV 2D2C performances for turbulence measurements. Then we discuss the precise experimental characterisation of the turbulence in our flow configuration and the first results obtained for the dispersed particle phase.

2. EXPERIMENTAL SET-UP AND DEVELOPMENT OF MEASUREMENTS METHODS

2.1 Experimental set-up and techniques

The experimental set-up (figure 1) has been defined to study the interactions between solid particles and turbulent gas flow with flow conditions allowing to vary the Stokes number in a wide range (cf. §3). We selected an original flow created by an axisymmetric jet confined in a tube. The interest of this flow (Risso *et al*., 1997) is to create a zone where the isotropy and a plane homogeneity are achieved around the tube axis and where the average flow is negligible in front of the velocity fluctuations. An original particles seeding system was developed in order to maintain an homogenous and stationary injection of glass particles (40-50µm of diameter). This system is constituted of a vibrating plate with holes of 500µm diameter and allows the solid particles injection by the top of tube in the turbulent flow. The solid flow rate is measured continuously by short time response balance. The experimental conditions of our runs are given in table 1.

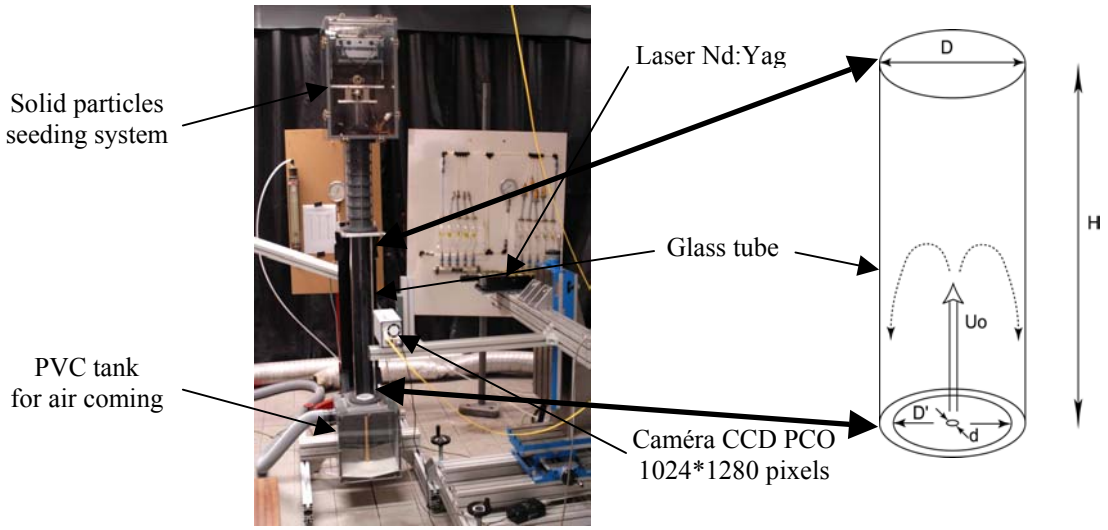

Experimental parameters: H=0.8m, D=0.1 m, D'=0.09 m, d=0.01 m, U_o=58m/s

Fig. 1. The experimental set-up

	U_0 (m/s)	Q_p (mg/s)
Run 1	58	0
Run 2	0	15
Run 3	58	22

Experimental conditions : $40\mu m<d_p<50\mu m$, $\rho_p=2400\ kg/m^3$, $Re_p=0.45$
Velocity at the jet inlet : U_o , diameter of the jet : d, kinematic viscosity of air: ν_{air}; $Re=Uod/\nu_{air}=38700$;
For $5<z/D<5.5$: Taylor micro-scale Reynolds number $Re_\lambda=60$ to 40
Turbulent Reynolds number based on the integral scale $Re_t=200$ to 100

Table 1. Experimental conditions

For each experimental run, we used a 2×30mJ 2ω Nd:Yag laser, a 1024×1280 pixels PCO CCD Sensicam camera. The flow is seeded by oil tracers (1-2µm of diameter) and PIV 2D2C is employed for gas velocity fields characterisation. We develop a PIV/PTV algorithm to measure simultaneously the velocity fields of both phases: gas flow and dispersed solid particles flow. In a preliminary stage, we focused on a study in order to validate PIV 2D2C measurements for homogeneous isotropic turbulent flow i.e. 2D velocity measurements in a 3D turbulent flow.

2.2 Performances of PIV measurements for homogeneous isotropic turbulent flow

In this section, we present a study of the effects of some parameters and turbulence characteristics on PIV velocity measurements following the same tests of Europiv (Lecordier *et al*., 2003). We used the PIV software developed by Maurel (2001). This software can calculate PIV with different algorithms and various optional functions as cell shifting, rotation and cell deformation. We have made gradual testing of the PIV. At first, we have analysed synthetic images in order to learn the limits of PIV measurements and to optimise the various options and parameters of the algorithm. Then, we have studied more realistic images with background noise. The effects of the different parameters on the velocity spectrum are discussed. We focussed on the spectrum estimation because the physical problem that we want to study is strongly dependent on the various scales of turbulence that we must characterise precisely.
The synthetic images (1032×1032 pixels size) were created by an original image particle generator developed at IMFT. This software creates synthetic image from a 2D or 3D velocity field and takes into account seeding diameter, time between frames, laser sheet energy, focal length, noise…. For this study, the velocity fields were obtained by 3D DNS (128^3) in a two phase flow with homogeneous isotropic turbulence for the gas phase (Fede *et al.,* 2004). The smallest length scales of the DNS homogeneous isotropic turbulence have an equivalent size of 8 pixels in synthetic images.

At first, we used synthetic images generated with a 2D flow without background noise and with a constant laser sheet energy simulated with a top hat shape. This test aimed to determine the first optimal parameters for PIV measurements like algorithm, mesh size, seeding diameter and concentration.
The algorithm including an iterative multigrid method with cell shifting and deformation gave the best results for the PIV energy spectrum as compared to DNS spectrum. There is no cut off of the spectrum for high wave numbers, and DNS and PIV spectra are identical. The other algorithm were not satisfactory in our homogeneous isotropic turbulent flow to obtain the velocity gradients.
We also examined the influence of mesh size for the first and second passes of PIV algorithm. It is essential to carry out 2 passes for the optimisation of PIV calculation, but the mesh size for the first pass is also very important and must be adapted to the mean seeding displacement. Carefully choosing an optimal first pass (32*32 pixels if not precised) we have studied the influence of the mesh size of the second pass: the small length scales are better resolved when mesh size for the second pass is as small as possible (figure 2). Afterwards, we used 8×8 pixels mesh size without recover.
Then, different tests have been carried out to analyse the effects of image seeding. We observed that it is essential to choose seeding with tracers whose image diameters are superior or equal to 2 pixels. For diameters inferior to 2 pixels, the energy spectrum was overestimated for high wave numbers. This effect is due to peak-locking phenomenon commonly observed for small size seeding. Concerning the seeding concentration, we noticed on figure 3 that the energy spectrum is well resolved if the number of tracers by mesh is greater or equal to 15 in the synthetic image as in Adrian study (1991).

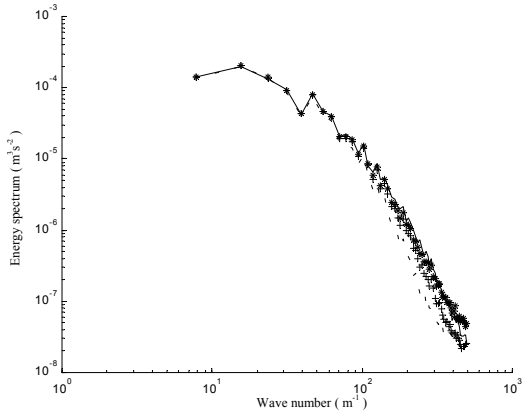

Fig. 2.Effect of mesh size for the second pass on the PIV calculation

—	DNS data
- -	mesh size : 32×32 pixels, 75% of recover
+	mesh size : 16×16 pixels, 50% of recover
*	mesh size : 8×8 pixels, without recover

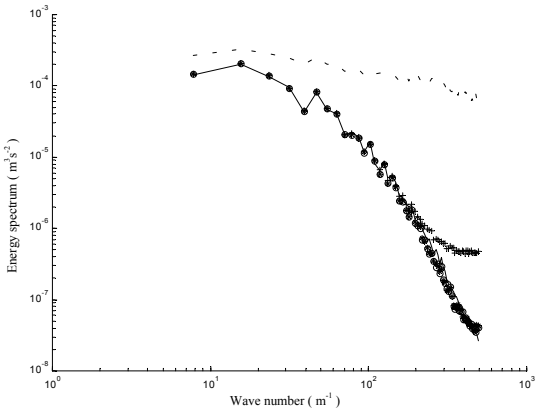

Fig. 3. Effect of seeding concentration on the PIV calculation

—	DNS data
- -	tracers number by mesh: 3/5
+	tracers number by mesh: 3
*	tracers number by mesh: 15
o	tracers number by mesh: 30

We also studied the effect of the amplitude of displacement between the two frames. In order to vary this amplitude we changed the "time delay" between the two frames, keeping the DNS velocity unchanged over a longer delay. The figure 4 shows the various energy spectra obtained. For lower and higher displacements, we can notice that the energy spectrum is overestimated for high wave numbers. In the first case, for small displacements, the accuracy of the algorithm (0.01 pixel) is of the same order as the displacement measured. On the contrary, for the higher times, the seeding displacements are too high as compared to the mesh size of PIV calculation and tracers are mislaid between the two frames. In this case, for the same reason, the energy spectrum is underestimated for low wave numbers. When we increase the seeding displacement (displacement greater than ¼ of the first cell), we mislaid more and more information about the largest structures of the flow. Thus, we decided to choose an intermediate mean displacement equal to 3 pixels which allows to obtain a good energy spectrum as compared to DNS spectrum.

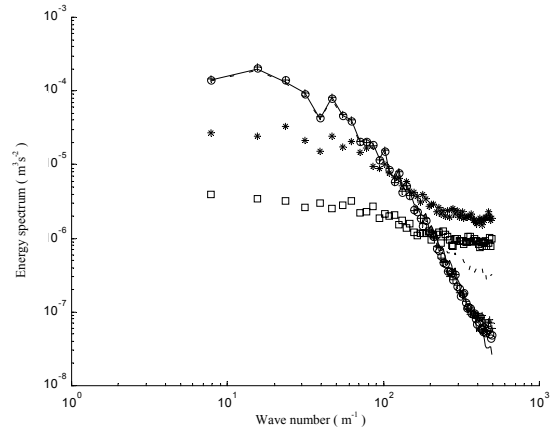

Fig. 4.Effect of seeding displacement on the PIV calculation

—	DNS data		
- -	0.14 pixels	o	2.70 pixels
*	6.75 pixels	□	13.50 pixels

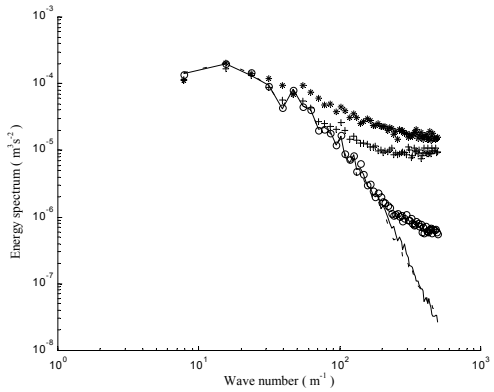

Fig. 5. Effect of ratio d/e on the PIV calculation

—	*DNS data*		
- -	d/e=¼	o	d/e=1
+	d/e=3	*	d/e=12

Finally, we studied the influence of the displacement perpendicular to the laser sheet for various energy profile shapes by means of synthetic images generated with a 3D flow without added noise. At first, we tested the effect of the projection of a non-coplanar motion on the CCD for a top-hat profile ; then we examined the influence of 3D motions on the persistence and changes of the images of the tracers in the laser sheet. We first tested the reference case of motions parallel to the laser sheet with a gaussian shape ; then we tested, for a Gaussian shape, the effect of the ratio between the width of the laser sheet e and the perpendicular displacement d between 2 frames.

For the top hat shape the third component velocity has few effect on the PIV calculation. The same result is observed with a gaussian shape without a third component velocity. On the other hand, on figure 5 we have reported the influence upon the energy spectrum of the parameter d/e for the more realistic case with third component and Gaussian shape. For the same laser sheet energy of gaussian shape, the best energy spectrum is obtained for a small ratio d/e. For the same third component velocity, the best energy spectrum is obtained for the higher thickness of laser sheet energy.

Finally, the last parametric study concerned the PIV calculation for the gas phase in a two-phase turbulent flows. This test is a preliminary study necessary to develop the PIV/PTV algorithm for two-phase flows (§2.3).

We created synthetic images more similar to real images: we added on the synthetic images already studied some random noise and "holes" representing the solid particles of the dispersed phase, that are supposed to have been detected and rejected from the images before PIV calculation (see § 2.3). Due to noise a lot of information for high wave numbers may be lost. Indeed, the seeding on the image has the same grey levels as the noise and during the PIV calculation, tracers and noise are not differentiated. We have tested the shape and size effects of the "holes" (figure 6) and we observed, as anticipated, that the smaller holes give the best energy spectrum as compared to the DNS one. For a ratio of the hole diameter to the mesh size of about 6/8 the deviation form the DNS spectrum is very important. In our experimental case, the particles images sizes will be of about 6 pixel. As denoted on figure 6, for such particles diameter, mesh size of 8x8 pixel for PIV calculations would thus induce too high bias in spectral estimations. Therefore we will choose 16x16 pixels mesh size with 50% recover to carry out the PIV calculation with real images. At the moment, images recorded in the experimental set-up for two-phase runs have not been processed. But single-phase flows were processed with 16x16 pixel sizes in order to prepare future comparison of the gas dynamics between the single-phase and the two-phase runs. We also examined the influence of the noise chosen to fill the holes on PIV calculation. Figure 7 shows that results are quite insensitive to a uniform random noise. To finish, we evaluated the influence of the mass loading on the quality of the PIV estimation. We can observe on figure 8 that energy spectrum is better resolved for low particles numbers, particularly for the high wave numbers. In our experimental set-up, we will have similar particle numbers (about 300/image). Measurement limitations thus induce a loss of a part of the small scales physics.

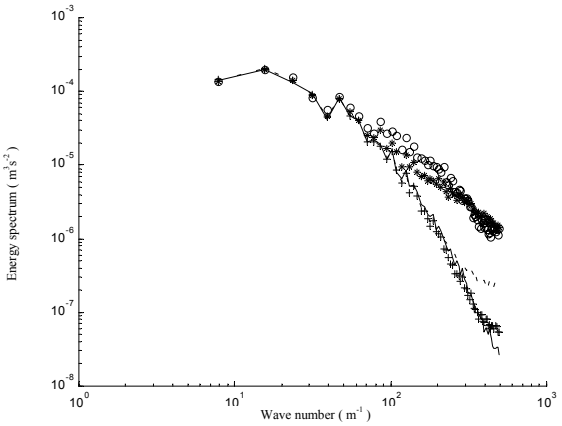

Fig. 6 Effect of shape and size of the inclusions on the PIV calculation (8×8 pixels mesh size without recover)

— DNS data
- - shape: square, size: 2 pixels
+ shape: circle, size: 2 pixels
o shape: square,size: 6 pixels
* shape: circle, size: 6 pixels

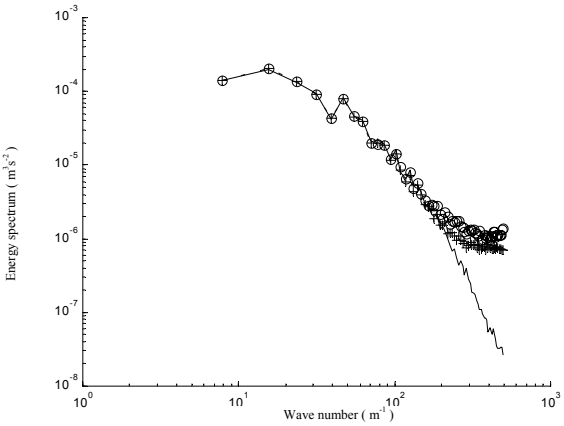

Fig. 7.Effect of noise in the inclusions (ratio between the noise amplitude and mean gray level of image) on the PIV calculation (16×16 pixels mesh size with 50% recover)

— DNS data
- - 0% of noise
+ 20% of noise
o 60% of noise

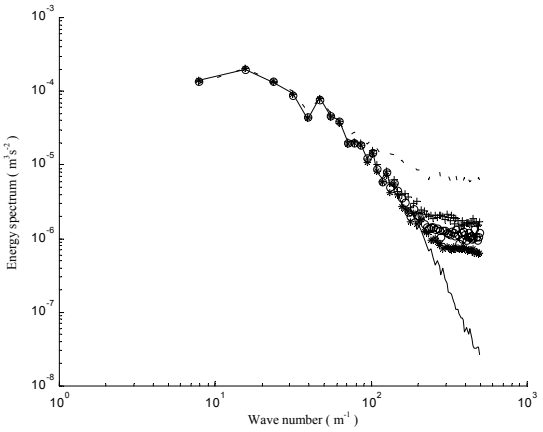

Fig. 8.Effect of inclusions number on the PIV calculation (16×16 pixels mesh size with 50% recover)

— DNS data

- - 900 inclusions/image + 300 inclusions/image

o 200 inclusions/image * 100 inclusions/image

2.3 Development of PTV technique

Particle velocity can not be measured with a PIV algorithm because particle density is too low (Adrian, 1991). So we developed a particle tracking velocity (PTV) algorithm more precisely described in Vignal *et al.* (2004). This algorithm can be separated in three different operations. The first is a phase separation, this separation is achieved with a local threshold function applied to the intensity of the image. After this stage, particles are detected and centers of all particles are calculated with a mass center method. The equivalent diameters are calculated at this stage. The second operation is the particle pairing between two families of particles detected in each frame. For a more accurate pairing, we make a preliminary PIV measurement in a large mesh (128*128 pixels) to give the approximated velocity. From its direction and intensity, we focus on a displaced window, and search the best pairing of all particles in this interrogation window (20x20 pixels). The pairing is based on a minimization of velocity variances in this interrogation window. After this particle pairing, precise velocity is calculated by cross-correlation of small regions around particle images (commonly 8*8 pixels). Preliminary tests with synthetic images give promising precision of the PTV algorithm, of about 0.1 pixel.

The last operation necessary to prepare PIV for gas phase is the suppression of the particles on the both frames: we replace particles by circles with random value functions of the mean intensity of the image. Figure 9 shows an example of the velocity fields of the two phases calculated by the PIV/PTV software with a two phase flow image. It shows promising tendencies.

From the results obtained in this section, we learnt how to fix the optimal experimental parameters for PIV/PTV measurements. This study was necessary to improve the quality of experimental results.

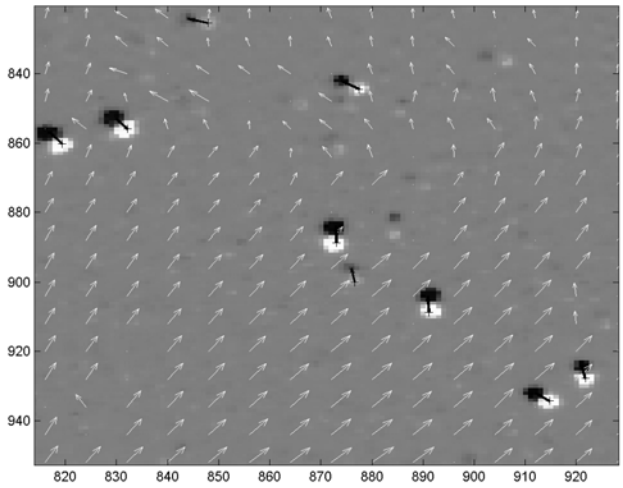

Fig. 9. Example of velocity fields calculated by the PIV/PTV software with a two phase flow image

White arrows: gas velocities
Black arrows: particle velocity

O: particles in the first frame

●: particles in the second frame

3. RESULTS AND DISCUSSION

In this section we present some new experimental results obtained in three distinct flow configurations (table 1). At first we have explored a single-phase case. Its dynamic is supposed identical to the carrier phase dynamic of the two-phase flow because the diameter of the particles is small in comparison with the Kolmogorov micro-scale of turbulence, and because the mass loading is chosen small enough so that there is no two-way coupling. We can thus consider that single-phase flow measurements give non-conditional statistics of the gas phase in the dispersed particle flow. The second case of study is the free falling of particles in the set-up, with no gas flow rate (run 2). It is the reference case for the dynamics of the particles. It allows to characterise the particles injection system. Then we present some preliminary results concerning the velocity field of the particle in a turbulent two-phase flow (run 3).
3000 PIV images are collected for each run at a frequency equal to 4 PIV images/second. This ensured statistical convergence, and independence of the samples (the integral time scale being of about 0.1s). The optics were adjusted as to optimise the tracer image diameter. The time delay between laser pulses is $800\mu s<\Delta t<1214\mu s$ in order to optimise the seeding displacement (lower than 8 pixels). The mesh size was 16x16 pixels. The statistics of the particles were also converged because there was about 300 particles/image.

3.1 Hydrodynamics of the carrier gas phase

The turbulence in the confined jet has been studied into details by Risso & Fabre (1997). These authors have shown that this flow configuration, even if quite complex, is interesting because there exists a region, far from the inlet, where the turbulence is isotropic at least up to second order moments, and homogeneous in the radial direction, with a slow evolution in the axial direction.

3.1.1 Global structure of the confined jet

The longitudinal evolution of the statistics of the velocity of the gas on the axis denotes the existence of 3 main distinct regions in the confined jet :

(1) up to z/D=2, the region of jet expansion, where the axial velocity decreases. This expansion is affected by confinement so that the rate of decrease is higher than for a free jet. The intense shear stresses produce an important amount of turbulence, and, in this region of production, the turbulence is not isotropic.

(2) from z/D=2 to z/D=4.4, a region of deep re-organisation, where the mean flow direction is reversed, and both axial and radial RMS velocities are damped but at a lower rate than the rate of attenuation of the mean velocity. Redistribution by turbulence leads to equalisation of the RMS velocities above z/D=4.4.

(3) above z/D=4.4, the region of interest for our study, described in the following paragraph.

A more detailed comparison with the results of Risso & Fabre (1997) shows that the different confinement parameter that characterises our set-up (α=d/D=0.1, and α=0.2 in Risso & Fabre) does not change the global structure of the flow, neither the lower limit of the region where turbulence is isotropic (z/D=4.4).

3.1.2 Turbulence characterisation in the region of diffusive turbulence

We have made precise measurements in the region 5<z/D<5.5. According to Risso & Fabre (1997), we have observed that the turbulent intensity is very important (200 to 300 %), and that isotropy (up to second order moments) and homogeneity around the axis of the tube in the radial direction (r/D<0.15) are achieved and maintained above z/D=4.4 (see figure 10). An evolution in the longitudinal direction remains, the mean flow and turbulence being attenuated in the direction of the top of the tube.
Another specific property of this flow is that the Eulerian integral length scale of turbulence is constant in this region where turbulence evolves only due to diffusion. The longitudinal integral length scale is L_{zz}=0.28D and the lateral one L_{zr}=0.1D.

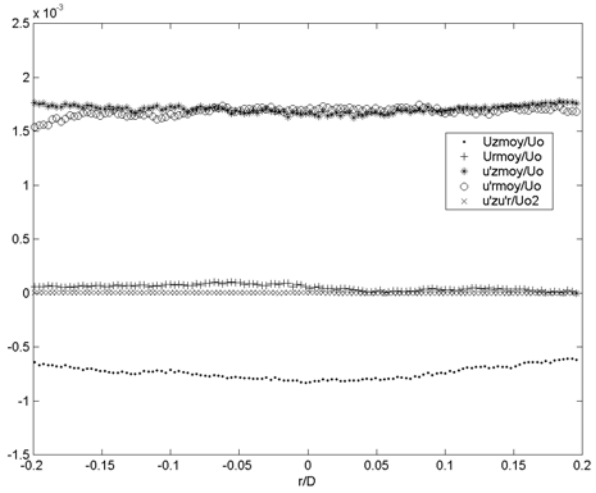

Fig. 10. Transverse profiles of the gas velocity moments of order 1 and 2 for z/D=5.3

3.2 First results about the dynamics of the particles

We have performed measurements of the velocity of the particles in the region of diffusive turbulence (5<z/D<5.5).
Two parameters can describe the time scale and velocity scale of the motion of a particle : its response time $\tau_p=\rho_p d_p^2/18\mu_{air}$ and its terminal velocity $U_{R\infty}$. The Reynolds number of the turbulence $Re_t=u_z'.L_{zz}/\nu$ varies between 200 and 100 for 5.<z/D<5.5. The continuous spectrum of time and velocity scales of turbulence may be crudely characterised by the integral length scale L_{zz}, the RMS velocity u_z' and the Kolmogorov micro-scales.
We can therefore define the following non dimensional numbers characteristic of the response of the particles to turbulence.
At first, from the single-phase experiments, we have estimated the Stokes number of the particles. We have defined two distinct Stokes numbers : one based on Kolmogorov scales, and the other based on the integral scales. The definition of both Stokes numbers is explained by the actual discussion about the scales responsible for the occurrence of the specific regime of inertial response leading to preferential concentration (some authors propose small scales (Fessler *et al.*, 1994, …), while others explain this occurrence through large scale mechanisms (Février, 2000, …)).
The Stokes numbers are defined as : $St_K=\tau_p/\tau_K$ and $St=\tau_p / T_L$, where the Kolmogorov time scale is $\tau_K=(\nu_{air}L_{zz}/u_z'^3)^{1/2}$, and T_L the Lagrangian integral time scale of the turbulence of the gas. We assume $T_L=0.8*T_e$ (Février, 2000) where T_e is the eddy turnover time ($T_e=L_{zz}/u_z'$). For run 3 and 5<z/D<5.5: St is always lower than 0.1, and St_K decreases from 1.1 to 0.5.
Then, the other parameter governing the particles dynamics is the ratio between the terminal relative velocity and the RMS velocity of the gas : $U_{R\infty}/u_z'$. In our experimental conditions of run 3, from z/D=5 to 5.5 it varies between 0.7 and 1.4. The crossing trajectories effects will thus be important in our experimental conditions (Csanady, 1963; Deutsh & Simonin, 1991).

3.2.1 Clustering of particles

In the range of Stokes numbers that we observed, preferential concentration may occur. That is, strong inhomogeneities in the concentration field can be generated by inertial mechanisms, heavy particles being preferentially ejected in the outward direction of the vortices by centrifugal forces. It is important to detect the appearance of this phenomenon because its effects may be strong enough to modify the relative movement or the turbulent dispersion (Eaton & Fessler, 1994,…). In order to discuss the occurrence of preferential concentration in our flow, we have performed the calculus of the number of particles density distribution. Following Fessler *et al.* (1994), we have divided our images into a regular grid of square boxes (32x32 or 256x256 pixels), and we have calculated the number of particles per box. We can observe, for the two runs and boxes of 32x32 pixels for the regular grid, that on the average the agreement with a Poisson law is good (figure 11-a). For the turbulent two-phase flow (run 3), and boxes of size equal to 256 pixels the measured density of probability of the number of particles in a box is different from the Poisson law that would be expected if the particles were randomly distributed across the flow (figure 11-b). We thus expect significant departure from randomness to occur. At the moment, it is not clear if such a departure is really due to inertial response of the particles to turbulence. While the Stokes numbers are in the range of values for which preferential concentration has been observed (St_K of order 1, St of order 0.1), it remains that for the free falling (run 2) such a departure is also observed, so that it is difficult to eliminate the eventual influence of any default of the injection system.

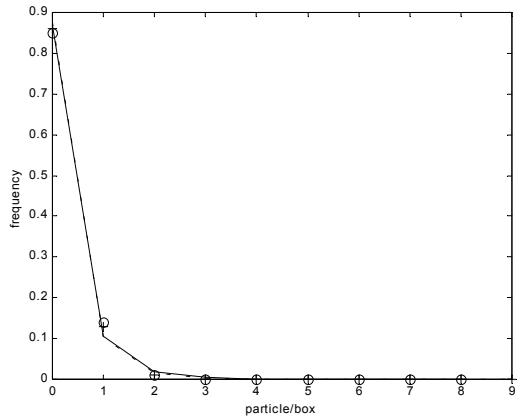

Fig. 11a. Particle number density for boxes of size 32x32 pixels

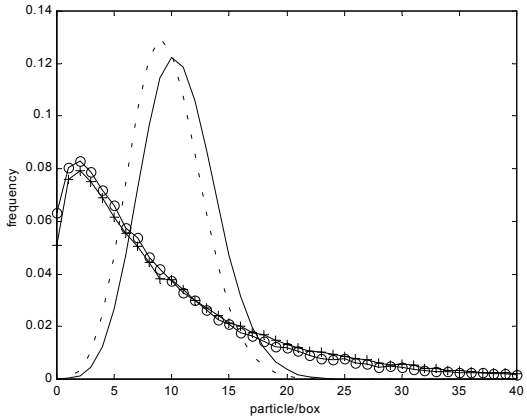

Fig. 11b. Particle number density for boxes of size 256x256 pixels

○ : run 3 continuous line : Poisson law for run 3

+ : run 2 dashed line : Poisson law for run 2

3.2.2 Enhancement of the settling velocity

The transverse profiles of the mean velocities of the particles for both runs 2 & 3, show that the actual particle injection system is not perfect. Some results show promising tendencies (see figure 12): the transverse velocities are always negligible as compared to the longitudinal one ; for the free falling, the mean relative velocity is near 0.1 m/s, a value in relative agreement with $U_{R\infty}$=0.14 m/s the terminal velocity of a particle of mean diameter equal to 45μm which is in the range of our particles diameters. Moreover, the whole profiles of particle longitudinal velocities are sensitive to the longitudinal acceleration of the fluid. Therefore, while the profiles at z/D=5.1 and 5.4 differ for run 3 because the fluid is accelerated, there is no difference between the profiles at z/D=5 and 5.4 for run 2 because there is no fluid motion. It remains that the injection system generates a non homogeneous longitudinal velocity profile in the transverse direction. We will ameliorate this system for definitive analysis.

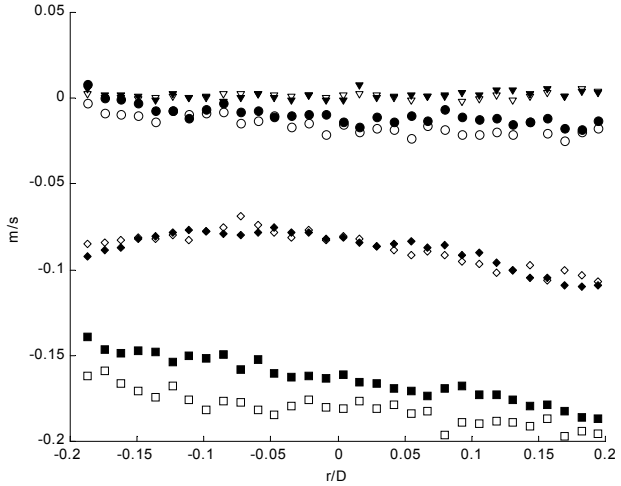

Fig. 12. Radial profiles of the mean velocities of the particles in runs 2 and 3

Particle longitudinal velocity $\overline{U_{zp}}$ *:* ◊ *run 2, 5<z/D<5.1* ♦ *run 2, 5.4<z/D<5.5*; □ *run 3, 5.1<z/D<5.2* ■ *run 3, 5.4<z/D<5.5*

Particle transverse velocity $\overline{U_{yp}}$ *:* ∇ *run 2, 5<z/D< 5.1* ▼ *run 2, 5.4<z/D< 5.5*; ○ *run 3, 5.1<z/D< 5.2* ● *run 3, 5.4<z/D<5.5*

In order to discuss the present dynamics of the relative motion, we have reported on figure 13 the longitudinal evolution of the mean velocities integrated across the transverse direction for the dispersed particle phase (across the extend of the window of observation where the gas flow was quite homogeneous (r/D<0.2)). While it is confirmed that the mean motion is vertical for both runs (2 and 3), and that there is no acceleration of the relative motion in the free falling case, the comparison of the longitudinal evolutions of $\overline{U_{zg}}$ and $\overline{U_{zp}}$ for the two-phase run 3 reveals a small acceleration of this relative motion during the fall ($U_R = \overline{U_{zp}} - \overline{U_{zg}}$ varies between 0.15 m/s and 0.17 m/s for z/D= 5.5 to 5). The fact that turbulence globally increases the mean settling velocity of the particles is in agreement with previous studies (Wang & Maxey, 1993; Février, 2000; Aliseda *et al.*, 2002). In our flow conditions, the ratio $U_{R\infty}/u_z$' evolves during the fall of the particles, and it will be interesting to discuss the modification of the mean relative velocity $\frac{(U_R - U_{R\infty})}{u'_z}$ as a function of Re_λ and St_K (see table 2).

Z/D	Re_λ	St_K	St	u'_z (m/s)	U_R (m/s)	$\frac{(U_R - U_{R\infty})}{u'_z}$ exp.
5	60	1.1	0.09	0.128	0.17	0.23
5.5	45	0.5	0.05	0.077	0.15	0.13

Table 2

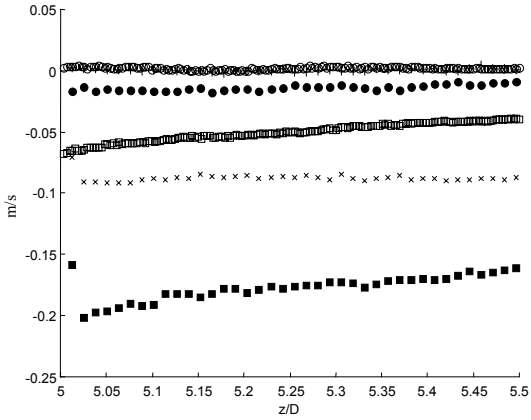

Fig. 13. Longitudinal evolution of the mean velocities

Run 1 : □ $\overline{U_{zg}}$ *;* ○ $\overline{U_{yg}}$ *; run 2:* x $\overline{U_{zp}}$ *;* + $\overline{U_{yp}}$ *; run 3 :* ■ $\overline{U_{zp}}$ *;* • $\overline{U_{yp}}$

3.2.3 Particle dispersion

The transverse profiles of the second order moments of the velocities of the particles are plotted on figure 14. The turbulent motions of the particles are less influenced by non homogeneity than the mean motion. Under data scattering, the shear stress is equal to zero for the free falling, and very low for the turbulent two-phase run 3. The longitudinal RMS velocity is always greater than the radial one, as well in run 2 as in run 3 due to the deviation from isotropy introduced by gravity effects. The more important energetic level obtained in run 3 is due to turbulent dispersion.

In order to analyse this turbulent dispersion, we have reported on figure 15 the longitudinal evolution of the RMS velocities of the gas and of the particles integrated across the transverse direction for the dispersed particle phase. The persistence of the isotropy of the turbulent velocity field of the gas over the region 5<z/D<5.5 is clearly denoted by the superposition of the curves of $\overline{u'^2_{zg}}$ and $\overline{u'^2_{rg}}$. The slowly attenuated values of $\overline{u'^2_{zp}}$ and $\overline{u'^2_{rp}}$ in run 2 give the reference agitation of the dispersed phase generated by the system of injection. In the turbulent dispersed flow, there is no isotropy of the turbulent motions of the particles. The less important level of the kinetic energy in the direction perpendicular to the crossing trajectory direction (aligned with the gravity acceleration), as compared to the level of the longitudinal energy is consistent with the extension of Tchen's theory when a slip velocity is present (Deutsch, 1992). But the ratio between the RMS velocity of both phases is quite important, and cannot be compared with the value predicted by this theory in isotropic and homogeneous turbulence. The influence of the level of the fluctuating motion of the particles at the inlet is thus non negligible. Complementary experimental studies will be devoted to an exploration of a region of greater longitudinal extension. Further analysis will be devoted to the role of advection, production, and turbulent diffusion in the determination of the longitudinal evolution of the particle kinetic stress tensor (Simonin *et al*., 1995).

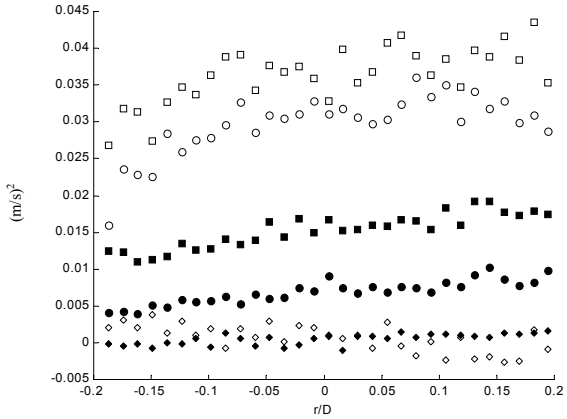

Fig. 14. Radial profiles of the velocity variances and shear stress of the particles in runs 2 and 3.

Run 2, 5<z/D<5.1 : ■ $\overline{u'^2_{zp}}$, ● $\overline{u'^2_{rp}}$, ♦ $\overline{u'_r\,u'_{zp}}$. *Run 3, 5.1<z/D<5.2 :* □ $\overline{u'^2_{zp}}$, ○ $\overline{u'^2_{rp}}$, ◊ $\overline{u'_r\,u'_{zp}}$.

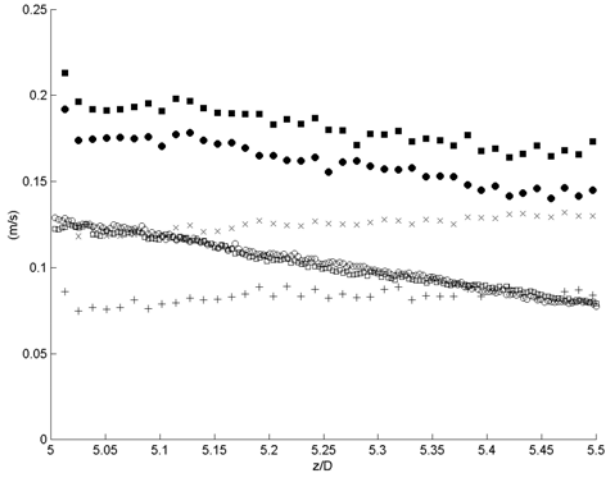

Fig. 15 Longitudinal evolution of the RMS velocities

Run 1 : □ $\sqrt{\overline{u'^2_{zg}}}$, ○ $\sqrt{\overline{u'^2_{rg}}}$; *run 2 :* x $\sqrt{\overline{u'^2_{zp}}}$, + $\sqrt{\overline{u'^2_{rp}}}$; *run 3 :* ■ $\sqrt{\overline{u'^2_{zp}}}$, ● $\sqrt{\overline{u'^2_{rp}}}$.

4. CONCLUSION

We developed a PIV/PTV algorithm to measure simultaneously the velocity fields of gas flow and dispersed solid particles flow. We focused, in the first part of this article, on the accurate validation of PIV/PTV technique to measure without bias the velocity fields of both phases for homogeneous isotropic turbulent flow. In this work we want to achieve accurate measurements with the PIV 2D2C technique. There are several difficulties to be resolved : at first the flow is turbulent and isotropic, that is strongly 3D, which is a difficult configuration for PIV measurements, then the flow will be a two-phase flow, with tracers to be distinguished from particles, and particles to be correctly removed before PIV calculation. Moreover, a large wave number range of the energy spectrum must be resolved in order to describe all the length scales of the flow. The first results for gas flow are in good agreement with the physics described in Risso (1997) (for more details of this study: Vignal *et al.*, 2003). Concerning the study of two-phase flow, we obtained promising preliminary results. According to these results, now, we need to improve the particles seeding system (in particular the homogeneity of particles injection).

REFERENCES

Adrian R. J. (1991). "Particle - Imaging techniques for experimental fluid mechanics." Annu. Rev. Fluid Mech. **23**: 261 - 304.

Aliseda A., Cartellier A., Hainaux F. and Lasheras J.C. (2002) "Effect of preferential concentration on the settling velocity of heavy particles in homogeneous isotropic turbulence". J. Fluid Mech. **468**: 77 – 105.

Csanady G.T. (1963). "Turbulent diffusion of heavy particles in the atmospere". J. Atmos. Sci. **20**: 201 – 208.

Deutsch E. and Simonin O. (1991). "Large eddy simulation applied to the motion of particles instationnary homogeneous fluid turbulence". In Turbulence Modification in Multiphase Flow, ASME-FED vol. 11: 35 – 42.

Deutsch E. (1992) "Dispersion de particules dans une turbulence homogène isotrope calculée par simulation numérique directe des grandes échelles". Thèse de l'Ecole centrale de Lyon, Collection des notes internes de la DER, Electricité de France, Clamart, France.

Eaton J. K. and Fessler J. R. (1994). "Preferential concentration of particles by turbulence." Int. J. Multiphase Flow **20** (Suppl.): 169 - 209.

Fede P., Février P. and Simonin O. (2004). "Numerical study of the effect of the fluid turbulence microscales on particle segregation and collision in gas-solid turbulent flows". 5th ICMF, Yokohama, Japan.

Fessler J. R., Kulick J. D. and Eaton J.K. (1994). "Preferential concentration of heavy particles in a turbulent channel flow." Phys. Fluids **6**(11): 3742 - 3749.

Février P. (2000). "Etude numérique des effets de concentration préférentielle et de corrélation spatiale entre vitesses de particules solides en turbulence homogène, isotrope, stationnaire". Thèse INPT. Toulouse, France.

Février P., Simonin O. and Legendre D. (2001). "Particle dispersion and preferential concentration dependence on turbulent Reynolds number from direct and large-eddy simulations of isotropic homogeneous turbulence". 4th International Conference on Multiphase Flow ICMF, New Orleans, Louisiana.

Khalitov D. A., Longmire E. K. (2002). "Simultaneous two-phase PIV by two-parameter phase discrimination". Volume 32, Number 2, pp. 252 – 268.

Lecordier B. and Trinité M. (2003). "Advanced PIV algorithms with windows deformation. Validation with synthetic images of turbulent flow". EUROPIV 2 Workshop on Particle Image Velocimetry, Zaragoza, Spain.

Maurel S. (2001). "Etude par imagerie laser de la génération et de la rupture d'un écoulement tourbillonaire compressé. Situation modèle pour la validation de simulations aux grandes échelles dans les moteurs". Thèse INPT. Toulouse, France.

Risso, F. (1994). "Déformation et rupture d'une bulle dans une turbulence diffusive". Thèse INPT. Toulouse, France.

Risso F. and Fabre J. (1997). "Diffusive turbulence in a confined jet experiment." J. Fluid Mech. **337**: 233 - 261.

Simonin O., Deutsch E. & Boivin M. (1995) "Comparison of large-eddy simulation and second-moment closure of particle fluctuating motion in two-phase turbulent shear flows". Turbulent Shear Flows **9**: 85 – 115, Springer-Verlag.

Squires K. and K. Eaton (1990)"Preferential concentration of particles by turbulence" Phys. Fluids **A3**(5):1169-1178.

Vignal L., Roig V., Ben L., Borée J. et Bazile R. (2003) "Une nouvelle installation expérimentale pour l'étude de la concentration préférentielle en écoulement gaz – particules solides", 16ème Congrès français de Mécanique CFM, Nice, France.

Vignal L., Ben L. et Cazin S. (à paraître septembre 2004) "Validation de mesures couplées PIV-PTV en écoulement turbulent diphasique gaz-particules", 9ème Congrès Francophone de Vélocimétrie Laser, Bruxelles, Belgique.

Wang L. P. and M. R. Maxey (1993). "Settling velocity and concentration distribution of heavy particles in homogeneous isotropic turbulence." J. Fluid Mech. **256**: 27 - 68.